Theoretical study of strain-induced ordering in cubic $In_xGa_{1-x}N$ epitaxial layers

L. K. Teles,[1,*] L. G. Ferreira,[2,†] L. M. R. Scolfaro,[1,‡] and J. R. Leite[1,§]
[1]*Instituto de Física, Universidade de São Paulo, Caixa Postal 66318, 05315-970 São Paulo, SP, Brazil*
[2]*Instituto de Física Gleb Wataghin, Universidade Estadual de Campinas, Caixa Postal 6165, 13083-970 Campinas, SP, Brazil*
(Received 12 January 2004; published 24 June 2004)

Chemical ordering in cubic epitaxial $In_xGa_{1-x}N$ layers is investigated by combining first-principles pseudopotential plane-wave total-energy calculations, a local concentration-dependent cluster-based method, and Monte Carlo simulations. It is found that for the unstrained or fully relaxed layers there are no stable ordered structures, indicating the tendency of the alloy to undergo phase separation, in agreement with previous calculations and experiment. The energetics of the $In_xGa_{1-x}N$ layers pseudomorphycally grown on fully relaxed GaN (001) buffers shows that biaxial strain acts as the driving force for chemical ordering in the alloys. It is found that strained $In_xGa_{1-x}N$ alloy comprises stable ordered structures which are (210)-oriented superlattices with composition in the range [0.5,0.63], the [AABB] alternation of planes (configuration "chalcopyrite") being the most stable phase.

DOI: 10.1103/PhysRevB.69.245317 PACS number(s): 61.66.Dk, 64.75.+g, 71.20.Nr, 71.22.+i

I. INTRODUCTION

In the past few years remarkable progress has been made in the development of optical and electronic devices based on group-III nitrides AlN, GaN, and InN and their alloys. Light-emitting diodes and laser diodes operating in the green-blue-UV spectral region and high-frequency, high-power, and high-temperature electronic devices have been successfully fabricated.[1–4] A common feature of these device structures is the use of ternary $In_xGa_{1-x}N$ or $Al_xGa_{1-x}N$ alloys. Alloying among the group-III nitrides allows one to change the band gap from 1.89 eV in InN to 6.28 eV in AlN with an intermediate value 3.44 eV for GaN (at 300 K).[5] Recently, a value of 0.7–0.9 eV was reported for the energy gap of InN, which allows an even wider range of variation for the band gap.[6,7] This feature can in principle be used in band-gap engineering of nitride-based systems.

Although these optoelectronic devices are produced commercially, the mechanism of light generation is still the subject of ongoing discussion. The controversy is due to the fact that the luminescence from GaN/InGaN/GaN quantum wells (QW's) is observed at energies significantly lower than the alloy band gap which is measured by absorption. The luminescence redshift has been explained to be due to excitons localized in indium-rich regions and it has been suggested that these regions are quantum dots (QD's) formed within the alloy matrix.[8,9] A quite different approach provides an explanation which does not require the presence of alloy composition fluctuations.[10] It has been proposed that the photoluminescence (PL) redshift in strained InGaN QW's originates from band tail states which are induced by piezoelectric and spontaneous polarization fields. In InGaN with cubic (c) crystal structure, contrary to the hexagonal (h) one, spontaneous polarization does not exist due to the higher crystal symmetry, and due to the (001) growth direction, strain-induced piezoelectric fields are negligible. Therefore, it has been recently suggested that investigations of c-InGaN QW's, which allows one to eliminate the modulation due to the spontaneous and strain-induced electric fields, are mandatory to understand the precise mechanism of light generation in InGaN-based optoelectronic devices.[11] The role played by In-rich QD's formed in c-InGaN layers on the light emission process has been observed from resonant Raman scattering experiments.[12] Unambiguous observation of light emission arising from QD's self-organized in h-InGaN active layers in multiple QW's has also been reported.[13] Recently, PL and high-resolution x-ray diffraction (HRXRD) experiments were combined to observe light emission from In-rich QD's in c-GaN/InGaN/GaN double heterostructures (DH's), grown on GaAs(001) substrates, with In content varying from $x=0.09$ to $x=0.33$.[14] The striking feature of the HRXRD reflexes is the fact that all the samples comprise In-rich QD's with In content of about $x=0.55$. It is interesting to observe that ordered $In_{0.5}Ga_{0.5}N$ domains of approximately 20 nm (QD's) were observed by transmission electron microscopy in h-$In_xGa_{1-x}N$ layers grown on (0001) saphire substrates with $x=0.25$ and $x=0.49$.[15]

Therefore, there now seems to exist enough evidence that self-organized QD's in InGaN layers are responsible for an important channel of light emission in nitride-based optoelectronic devices. The answers to the questions how these dots are formed, what are their structures and sizes, what are their electronic and optical properties are very important to improve on device performance and to extend the emission range to comprise longer wavelengths. Knowledge of the energetics and thermodynamic properties of the ternary InGaN alloy layers paves the way to answer those questions.

It is now known that the nitrides are not fully miscible; i.e., there are strong indications for a miscibility gap.[12,16,17] The large difference in the equilibrium lattice constants of InN and GaN (11%) results in a considerable internal strain and drives the tendency of phase separation, though phase separation suppression due to external biaxial strain was observed in InGaN alloy layers by HRXRD and Raman scattering spectroscopy.[18,19] Besides the phase separation process, chemical ordering on the group-III sublattice of InGaN has been reported.[15,20–22] It is already well known for various III-V semiconductors that long-range- or short-range-ordered

 ©2004 The American Physical Society

stoichiometric intersemiconductor compounds can be more stable than the disordered alloy below some growth temperature T_c.[23–25] Moreover, the coherence with the substrate can convert the previously metastable and unstable bulk ordering into stable epitaxial ordering.[26]

Despite the great importance and interest in the group-III nitrides and the fact that ordered phases were already experimentally observed, there is no systematic theoretical study of the existence of bulk ordered structures and the stability of them, as well as their relation with the biaxial strain. Recently, we investigated the possibility of occurrence of ordering in InGaN alloys based on an entirely different method requiring a small number of *ab initio* calculations. That method is expected to be less precise, although it leads to the same qualitative result as the present work.[27]

In this work, we present a rigorous and systematic theoretical study of the effect of biaxial strain on c-$In_xGa_{1-x}N$ alloys, and not only about the possibility of ordered phases formation, but also a detailed study of which is the most stable structure. In this sense, we reexamine the previous results by using another cluster expansion method with a larger number of configurations than in Ref. 27. We intend to simulate a fully relaxed alloy and a coherently grown alloy on top of a relaxed c-GaN(001) thick layer. Therefore, we consider a pseudobinary nitride alloy $In_xGa_{1-x}N$ which crystallizes nearly in a tetrahedrally coordinated lattice. We assume the cubic zinc-blende structure but our results can be qualitatively transferred to the hexagonal wurtzite or a tetragonal system. Explicitly, we will consider biaxially strained zinc-blende crystals in the direction of a cubic axis—i.e., tetragonal structures. The calculations performed here are based on an *ab initio* pseudopotential plane-wave method, within the framework of the density functional theory and the local density approximation, a concentration-dependent cluster-based model, and Monte Carlo (MC) simulations. The paper is organized as follows. In Sec. II we describe the details of the calculation methods. In Sec. III we discuss the alloy stability and the strain effect on the formation of ordered alloys. Finally, a summary is given in Sec. IV.

II. CALCULATION METHODS

The theoretical study of the alloy energetics and thermodynamics performed here requires several steps which we describe below.[25,28–30]

A. Cluster expansion

1. Traditional approach

A general approach to the energetics of substitutional systems is the cluster expansion (CE), in which the energies of the different configurations are described by a generalized Ising Hamiltonian.[24–26,31–34] In the CE one uses a given underlying lattice (fcc, bcc, etc.) and defines a configuration σ by specifying the occupation of each of the N lattice sites by, as in our case, an In or Ga atom. For each configuration, one assigns a set of fictitious spin variables $S_n (n=1,2,\ldots,N)$ to each of the N sites of the lattice ($S=-1$ for occupied Ga sites and $S=+1$ for In). The set of spin variables S_n defines the configuration σ. The energy of any configuration σ can be written as

$$E(\sigma) = J_0 + \sum_i J_i S_i(\sigma) + \sum_{j<i} J_{ij} S_i(\sigma) S_j(\sigma) + \sum_{k<j<i} J_{ijk} S_i(\sigma) S_j(\sigma) S_k(\sigma) + \cdots, \qquad (1)$$

where the J's are the interaction energies and the first summation is over all sites in the lattice, the second over all pairs of sites, the third over all triplets, and so on. These constitute the basic figures of the lattice. The interaction energies are the same for all configurations σ. Thus, if the J's are known, the energy $E(\sigma)$ for any σ can be calculated by simply calculating the spin products and summing, and one can readily find the ground-state structures,[24] as well as use statistical mechanics techniques such as MC simulations to calculate the thermodynamic properties of the alloy.

2. Modifying the cluster expansion

The CE is specially useful when it converges fast. In the case of nonmetals the Coulomb interaction $(1/r)$ and the elastic interaction between different sized atoms $(1/r^3)$ are long range and require far extended CE (or a different method, as Ewald's in the case of the Coulomb interaction). These long-ranged expansions—because the many parameters are obtained by fitting the configuration energies of a large set—present new dangers because wrong (or incomplete) long-range interactions may enhance the importance (nearness to the ground state) of wholly unphysical configurations. In the case of $In_xGa_{1-x}N$ we decided to use a relatively short-ranged novel CE but with a number of parameters larger than the usual short-range expansions, but sufficient to fit the energies of a large set of configurations with tolerable errors.

To present this novel CE we rewrite Eq. (1) as

$$E(\sigma) = \sum_f \sum_{n=1}^{N} \frac{1}{V_f} \sum_{k=1}^{V_f D_f} J_f S_n S_{f,k,2} \cdots S_{f,k,V_f}, \qquad (2)$$

where f means a figure-type (empty figure, point, pairs, triangles, etc.) with V_f vertices, one of which is the site n being summed. D_f is the number of figures of type f per site. In other words, we sum over all figures with a vertex at site n and then sum over all sites. Since there are D_f figures of type f per site and those figures have V_f vertices, the sum over the figures f with a vertex at n has $V_f D_f$ terms. The product $S_n S_{f,k,2} \cdots S_{f,k,V_f}$ means the product of spins at the V_f vertices of the kth figure f having one vertex at n. In this product, the spin of the second vertex of the figure is $S_{f,k,2}$ and the spin of the V_fth vertex is S_{f,k,V_f}.

Written as in Eq. (2) the CE can be readily generalized by making the interaction to be *site-dependent* through its "local concentration" $J_f(x_n)$. We postpone to the next subsection the definition of the local concentration. Now we observe that making the interactions dependent on the concentration x is not a new idea.[35] The procedure comes as necessary whenever the number of interactions, J_f, is small and the elastic interaction, due to the different atomic sizes, is important.

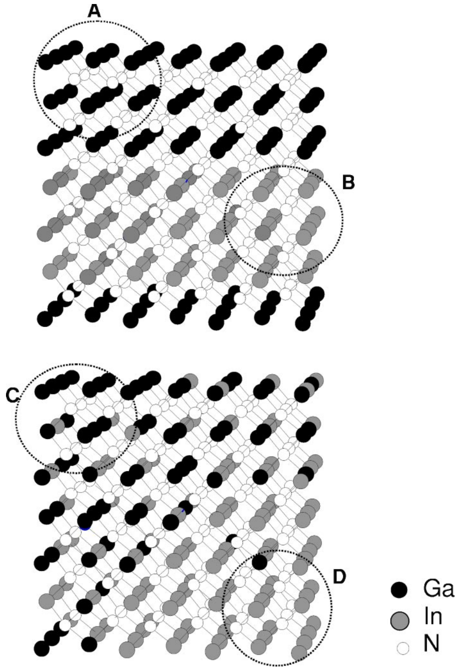

FIG. 1. Examples of InGaN alloys with regions (denoted by A, B, C, and D) with local compositions different from the average one.

For a general configuration we might use its global concentration to define the interactions J. But such a definition is inadequate for those configurations, like the long-period superlattices, having large domains of off-average concentration, as illustrated in Fig. 1. Considering this fact, we decided to make the J's dependent on the local concentration, which is defined as follows.

3. Defining the local concentration x_n

To define the local concentration x_n we consider the spin S_n of the site n of the cation fcc sublattice, the spins $S_n^{(1,l)}$ of the 12 sites of the first shell of neighbors ($l=1,\dots,12$), and the spins $S_n^{(2,m)}$ of the 6 sites of the second shell ($m=1,\dots,6$). The average spin at the site n and the local concentration are then defined, respectively, as

$$\bar{S}_n = \frac{r}{M}S_n + \frac{t}{M}\sum_{l=1}^{12} S_n^{(1,l)} + \frac{u}{M}\sum_{m=1}^{6} S_n^{(2,m)} \tag{3}$$

and

$$x_n = \frac{1}{2} + \frac{\bar{S}_n}{2}. \tag{4}$$

The parameters r, t, u, and M are unknown. Naturally they should be chosen so that, for the end compositions, GaN and InN, $x_n=0$ and $=1$, respectively. That sets

$$r + 12t + 6u = M. \tag{5}$$

For the very simple configurations $L1_0$ and $L1_1$ (for nomenclature see Ref. 36), we decided that the local concentration x_n *at all sites, Ga or In*, should equal the global concentration $x=1/2$. Then, normalizing the set of parameters, we obtain

$$r=6, \quad t=3, \quad u=1, \quad M=48. \tag{6}$$

It is a remarkable fact that, with this choice of parameters, the equality $x_{local}=x_{global}$ is also valid for all sites of the configurations $L1_2$, though Ga and In here occur at ratios 3:1 and 1:3.

4. Power series expansion of J

To arrive at a Hamiltonian linear with the fitting parameters, we expand the J's in a power series:

$$J_f(x_n) = \sum_{l=0}^{l_{max}} J_{f,l}(x_n - 0.5)^l = \sum_{l=0}^{l_{max}} 2^{-l} J_{f,l}\bar{S}_n^l. \tag{7}$$

Typically we will use a maximum power $l_{max}=2$ because the large powers are risky since they may enhance the importance of unphysical configurations. The Hamiltonian becomes

$$E(\sigma) = \sum_{l=0}^{l_{max}} 2^{-l}\left\{\sum_{n=1}^{N}\sum_{f}\frac{1}{V_f}\sum_{k=1}^{V_f D_f} J_{f,l}\bar{S}_n^l S_n S_{f,k,2}S_{f,k,3}\cdots S_{f,k,V_f}\right\}. \tag{8}$$

For a given set of first-principles-calculated configurations, we fit the Hamiltonian of Eq. (8) with fitting parameters $J_{f,l}$, instead of fitting the standard CE Hamiltonian with parameters J_f. Naturally, for an equivalent fitting quality, we will need fewer figures f and extend the interaction to a shorter range. Possibly this is the advantage of the new CE over the traditional approach, because, as explained before, an unbalanced set of long-range interactions affects an impossibly large number of configurations, about which we know very little, some being unphysical.

Another point to be discussed with respect to Eq. (8) is that, if all 2^N figures were included,[28] the series would be overcomplete. Of course, with fewer than 20 parameters $J_{f,l}$ there is no risk running into problems of overcompleteness.

B. First-principles calculation of the basic configurations

The total-energy and electronic structure calculations for each configuration to be used in the CE are based on the density functional theory (DFT) in the local density approximation (LDA).[37,38] Besides the valence electrons also the semicore Ga 3*d* and In 4*d* states are explicitly considered. Their interaction with the atomic cores is treated by non-norm-conserving *ab initio* Vanderbilt pseudopotentials.[39] As a consequence of the optimization, the plane-wave expansion of the single-particle eigenfunctions may be restricted to an energy cutoff of 22.2 Ry for all nitrides and their alloys. The cutoffs have been carefully tested in the case of bulk structures, cleaved and basal-plane surfaces.[40,41] However, to be on the safe side the cutoff is substantially increased, since in the ternary alloy case shorter bond lengths than that of the binary InN occur. The many-body electron-electron interaction is described within the Ceperley-Alder scheme as parametrized by Perdew and Zunger.[42] The **k**-space integrals

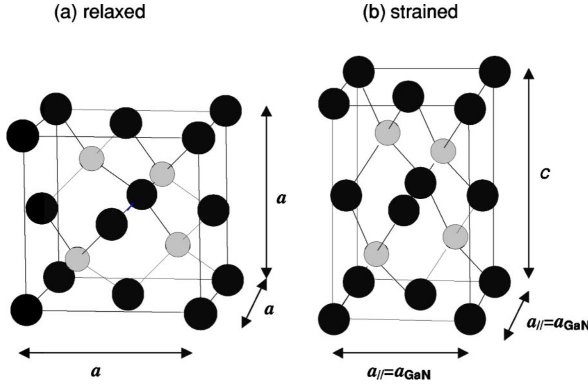

FIG. 2. Scheme of how the biaxial strain produced by the pseudomorphic growth of InGaN on GaN was taken into account in the calculations. (a) and (b) are two possible clusters with In, Ga atoms (black circles) and N atoms (gray circles). The presence of a possible biaxial strain perpendicular to the (001) direction is indicated by the two different lattice constants $a_{\parallel}$ and c.

are approximated by sums over a $5\times5\times5$ special points of the Monkhorst-Pack type within the irreducible part of the Brillouin zone.[43] Our calculations employ the conjugate-gradient method to minimize the total energy. Explicitly we use the so-called "Vienna *Ab initio* Simulation Package" (VASP).[44,45]

The InGaN alloys are usually grown on a buffer of GaN. Then, in order to determine the total energy of each configuration under the macroscopic strain produced by the pseudomorphic growth the lattice parameter in the plane (001), $a_{\parallel}$, was held fixed and equal to that of GaN. In Fig. 2 the biaxial strain produced by the coherent growth of InGaN layers on rigid GaN (001) buffers is schematically shown. Table I presents the LDA-calculated total energies for the configurations used in the cluster expansion. Most of the configurations in the table may be oriented in two ways with respect to the axis (001) perpendicular to the substrate. The configuration total energies were calculated as functions of the lattice parameter c along the (001) direction and minimized with respect to the atomic positions within the unit cell. The set of configurations are named as in Ref. 36 to which we add a fraction n/m, like 1/2 or 3/4, saying that among the m sites of the unit cell n are occupied by In and $m-n$ by Ga. The set of configurations includes *all* with two and four cations per unit cell (in Ref. 36 the configurations X were not calculated). The name of the configuration "40" (chalcopyrite) is here being changed into $DO_{22}2/4$ because it has the same unit vectors as DO_{22}. Since the lattice parameter in the basal plane was set equal to that of GaN, most configurations split into two, one mostly oriented in the (001) direction, the other mostly oriented perpendicularly. The configurations $L1_1$, V, and $L1_2$ do not split due to the lattice uniaxial deformation. Aside from the configurations with two and four cations/cell we also calculated $\gamma1$ and $\gamma2$ ($MoPt_2$), the superlattice [3,3] along the (001) direction, and a configuration with eight cations/cell which is an alternation of planes along the (001) direction: plane (AB), followed by plane (AA), followed by (BA), followed by (BB), and back to the beginning. This configuration may be thought as a $DO_{22}2/4$ ("40") with planes intercalated by those of $L1_0$.

TABLE I. LDA-calculated configuration energies (eV per 4 cations) for the configurations with planes of atoms mostly parallel ($E_{\parallel}$) and perpendicular ($E_{\perp}$) to the (001) direction and the respective weighted averages (E_{av}) (last column). Note that some configurations do not split due to the lattice uniaxial deformation. The entries of the last column were used for the least-squares fit of the CE. The configurations were denoted according to Ref. 36 with the addition of others defined in the text.

Configuration	$E_{\parallel}$(eV)	$E_{\perp}$(eV)	E_{av}(eV) $\frac{1}{3}E_{\parallel}+\frac{2}{3}E_{\perp}$
fcc0/1	–56.06286	–56.06286	–56.06286
fcc1/1	–47.96129	–47.96129	–47.96129
$L1_0 1/2$	–51.99649	–51.88802	–51.92070
$L1_1 1/2$	–51.67201	–51.67201	–51.67201
$\gamma1(MoPt_2 1/3)$	–53.46449	–53.43675	–53.44599
$\gamma2(MoPt_2 2/3)$	–50.74573	–50.69255	–50.71028
$Y1/4$	–53.84288	–53.95924	–53.92046
$Y3/4$	–49.98981	–49.82149	–49.97511
$Y2/4$	–52.00527	–52.03549	–52.02541
$Z1/4$	–54.00243	–53.97062	–53.98122
$Z3/4$	–49.94279	–49.85288	–49.88285
$Z2/4$	–52.01520	–51.88448	–51.92805
$X1/4$	–53.65886	–53.80402	–53.75563
$X3/4$	–49.82149	–49.79737	–49.80540
$W1/4$	–53.85239	–53.85478	–53.85398
$W3/4$	–49.93638	–49.90490	–49.91538
$W2/4$	–52.09681	–52.02756	–52.05064
$V1/4$	–53.74721	–53.74721	–53.74721
$V3/4$	–49.69583	–49.69583	–49.69583
$V2/4$	–51.65544	–51.65544	–51.65544
$L1_2 1/4$	–53.93242	–53.93242	–53.93242
$L1_2 3/4$	–49.95694	–49.95694	–49.95694
$DO_{22}1/4$	–53.85119	–53.86628	–53.86125
$DO_{22}3/4$	–50.03621	–50.07768	–50.06386
$DO_{22}2/4$	–52.08305	–52.20862	–52.16675
(AB)(AA)(BA)(BB)	–52.04565	–52.05774	–52.05371
[3,3]	–52.09600	–52.09600	–52.09600

C. Fitting the modified cluster expansion to first-principles data and making the ground-state search

The 27 entries of the last column of Table I were fit with the 15 parameters listed in Table II. The fitting error for the 27 entries of the last column was 10.5 meV/cation and for the 45 LDA calculated configurations was 14 meV/cation. We considered these errors small enough for our purposes. For comparison, in Table III we present the weighted averages of the LDA-calculated configuration energies, as in the last column of Table I, and the corresponding predicted energies from the CE.

The set of the obtained interaction energies J's is then used in the novel CE [Eq. (8)] to predict the energies of new configurations σ. This was made for a large set of 5868 configurations. Then, by using the same procedure as in Ref.

TABLE II. Interaction energies in units of eV/(4 cations). Here K stands for the second-neighbor pair interaction, L stands for the third neighbor, and M stands for the fourth neighbor.

$J_{0,0}$	−51.863 244 70
$J_{0,1}$	7.95599463
$J_{0,2}$	4.85742631
$J_{1,1}$	−2.78332746
$J_{2,0}$	0.84144467
$J_{2,2}$	−8.70087009
$J_{3,0}$	0.07249960
$J_{3,1}$	3.65899664
$J_{4,0}$	−0.04153010
$J_{4,2}$	−3.73237247
$K_{2,2}$	1.40625278
$L_{2,0}$	−0.33724278
$L_{2,2}$	2.46770814
$M_{2,0}$	0.14631820
$M_{2,2}$	−1.07510859

24 to identify those structures which minimize the energy expression at each x, we obtained the ground-state line (GSL), which is discussed in Sec. III. The GSL is made of straight line pieces in the plane ΔE versus x such that any configuration has energy greater or equal to the two phase mixtures corresponding to the straight pieces. ΔE is the standard definition of the alloy excess energy taken as the difference between the alloy energy and the mixture energy of the GaN and InN binaries, $\Delta E = E(\sigma) - [xE_{InN} + (1-x)E_{GaN}]$.

D. Using the modified cluster expansion in Monte Carlo runs to find the range of thermal stability

Having identified the ground-state structures, it remains to be seen whether the stability-limit temperature is sufficiently high to allow growth of these ordered phases. For this purpose, we constructed a MC program. Knowing the Hamiltonian, Eq. (8), defining the MC periodic cell, and choosing the temperature, one attempts switching spins between two sites, accepting the motion or refusing it according to the Metropolis recipe.[46]

The way we made the MC dynamics (spin switching between two sites) guaranteed that the concentration x remained fixed (canonical MC). The two sites were chosen among the 12 nearest neighbors of the first site. We made MC runs with a cell of unit vectors (0 12 12), (12 0 12), and (12 12 0). The fcc unit cell has (0 1 1), (1 0 1), and (1 1 0), and thus the MC cell contains $12^3 = 1728$ cations. As the MC sample is heated from perfect order at very low temperatures or cooled from disorder at high temperatures, the best way to follow the buildup or disappearance of order is by following the intensity of a "Bragg reflection" typical of the symmetry of the perfect ordered structure. We proceed in the following way. Let $S(\vec{l})$ be the spin (±1) at the fcc site $\vec{l}$. Consider the intensity $S(\vec{k})S(\vec{k})^*$ of the Fourier transform $S(\vec{k}) = \Sigma_{\vec{l}}\, S(\vec{l}) e^{i\vec{k}\cdot\vec{l}}$, where $\vec{k}$ is a reciprocal lattice vector. If there is ordering, then $\vec{k} = \vec{G}$, where $\vec{G}$ is a reciprocal lattice vector of the perfect ordered configuration, and the intensity of the Bragg reflexes is typically very large (proportional to N^2, with N the number of fcc sites in the MC cell). As the temperature increases the value of this "Bragg" intensity decreases by orders of magnitude. For other wave vectors $S(\vec{k})S(\vec{k})^*$ is small, but this background (diffuse scattering) increases as the temperature approaches the phase transition.

When the disordered phase is achieved, the Bragg intensity becomes proportional to the number of fcc sites in the MC cell, $S(\vec{k})S(\vec{k})^* \simeq N$. As the temperature increases, the intensity of the Bragg lines can have a discontinuous behavior, jumping to the diffuse scattering level, or it can decrease smoothly to the value for a disordered MC sample. When the behavior is discontinuous we have a first-order transition; when it is continuous we might have a second-order transition or the size of the MC sample is too small to detect a discontinuous behavior.

TABLE III. Weighted averages E_{av} of the LDA-calculated configuration energies (eV per 4 cations) of the configurations mostly parallel ($E_{\parallel}$) and perpendicular ($E_{\perp}$) to the (001) direction, as showed in the last column of Table I, and the corresponding predicted total energies from the CE, E_{CE}. The energies are given in eV per 8 atoms.

Configuration	E_{av}	E_{CE}
fcc0/1	−56.06286	−56.06116
fcc1/1	−47.96129	−47.96016
$L1_0 1/2$	−51.92070	−51.92652
$L1_1 1/2$	−51.67201	−51.67540
$\gamma 1(MoPt_2 1/3)$	−53.44599	−53.39984
$\gamma 2(MoPt_2 2/3)$	−50.71028	−50.79618
$Y1/4$	−53.92046	−53.89354
$Y3/4$	−49.97511	−49.91554
$Y2/4$	−52.02541	−51.97174
$Z1/4$	−53.98122	−53.98380
$Z3/4$	−49.88285	−49.93331
$Z2/4$	−51.92805	−51.96327
$X1/4$	−53.75563	−53.79834
$X3/4$	−49.80540	−49.82034
$W1/4$	−53.85398	−53.85315
$W3/4$	−49.91538	−49.87516
$W2/4$	−52.05064	−52.00349
$V1/4$	−53.74721	−53.77637
$V3/4$	−49.69583	−49.72587
$V2/4$	−51.65544	−51.64929
$L1_2 1/4$	−53.93242	−53.87588
$L1_2 3/4$	−49.95694	−49.97038
$DO_{22} 1/4$	−53.86125	−53.93166
$DO_{22} 3/4$	−50.06386	−50.02616
$DO_{22} 2/4$	−52.16675	−52.16980
(AB)(AA)(BA)(BB)	−52.05371	−52.11991
[3,3]	−52.09600	−52.02047

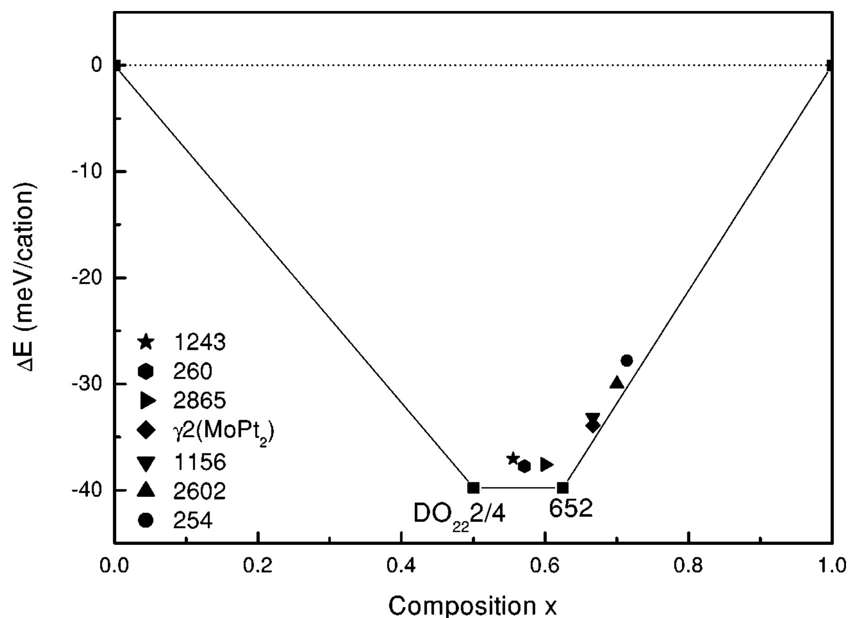

FIG. 3. Excess energy ΔE for some relevant ordered structures for the $In_xGa_{1-x}N$ alloy pseudomorphically grown on rigid GaN (001) buffer layers ($a_{\parallel}=a_{GaN}$). The solid curve gives the alloy ground-state line (GSL) and the dotted line connects the two binary GaN and InN constituents taken as the reference to calculate ΔE. The excess energies of ordered structures near the GSL are also represented. Note that the chalcopyrite structure $DO_{22}2/4$ always belongs to the GSL, being the most stable structure. The configurations are named, when known, according to the literature, when not, according to the sequence number of configuration in the file with the 5868 different configurations. If they are or not superlattices and their plane alternation are given in Table IV.

III. RESULTS AND DISCUSSION

During the epitaxial growth one introduces (i) coherence with the substrate at the film/substrate interface and (ii) a free surface at the film/vacuum interface. We described how epitaxial coherence alone, without surface effects, modifies the phase diagram of a bulk alloy. For other III-V alloys, various ordered structures were already observed in the literature, for which the first effect was enough to predict and describe them.[26] Our discussion will consider two forms of solids, the unstrained alloy, which is thick and "free standing" (without a substrate), and the strained alloy—i.e., a thin film without misfit dislocations grown epitaxially on a thick substrate. In this case the parallel dimensions of the film are determined by those of the substrate. It is also important to point out that we explored the thermodynamic consequences of the coherent epitaxy rather than its kinetic aspects. The only imposed kinetic limitation in the MC simulations was to restrict diffusion to the exchange of nearest-neighbor atoms.

We first investigated the relative stability of ordered and disordered phases, considering the coherent case for which $a_{\parallel}=a_{GaN}$. The resulting GSL is shown in Fig. 3, and as was explained before,[24] it consists of straight line pieces between some points which correspond to the stable ordered configurations of atoms. The GSL has two inflection points: the one at $x=0.5$ is $DO_{22}2/4$, as expected from the LDA calculation, which is a superlattice along the (210) axis with alternation of planes [InInGaGa], represented in Fig. 4; the second at $x=0.625$ is also a (210)-oriented superlattice with alternation [InInInGaInInGaGa].

Recently, as already mentioned before, we investigated the possibility of the occurrence of ordering in InGaN alloys, by using a less precise method, with a small number of *ab initio* calculations.[27] In that work[27] we restricted the cluster expansion to the figures J_0, J_1, J_{2in}, J_{2out}, J_3, and J_4, where J_{2in} is the first-neighbor pair interaction in a plane perpendicular to (001) and J_{2out} is the interaction outside the plane. We named and numbered these interactions sequentially as $J^{(j)}$ $(j=1,\ldots,6)$. At each perpendicular lattice parameter c we used the energies of six configurations to determine the concentration-dependent interactions $J^{(j)}(c)$ by matrix inversion. Since, following Vegard, c is a function of x, $c(x)$, the interactions resulted functions of x, $J^{(j)}(x)$. As in the present

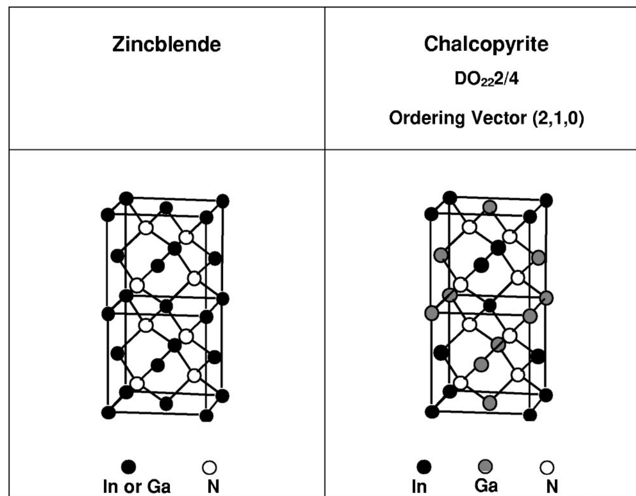

FIG. 4. Arrangement of atoms in the zinc-blende configuration compared to the chalcopyrite ($DO_{22}2/4$) configuration, which is the lowest in energy.

TABLE IV. Configurations with energy higher than the ground-state line (GSL) by no more than 3 meV/cation. The first column corresponds to the name of the respective configuration when it is known: when not, it correspond to the sequence number of the configuration in the file with the 5868 different configurations. Observe that the (210)-oriented superlattices that are competing have at most three consecutive planes B.

Configuration	x	Ordering vector	Plane alternation
$DO_{22}2/4$[a]	0.5	(2,1,0)	[*BBAA*]
1243	0.555555	(2,1,0)	[*BBBAABBAA*]
260	0.571429	(2,1,0)	[BBABBAA]
2865	0.6	Not a superlattice	
652[b]	0.625	(2,1,0)	[*BBBABBAA*]
$\gamma 2(MoPt_2)$[c]	0.666667	(2,1,0)	[*BBA*]
1156	0.666667	(3,1,0)	[*BBBBABABA*]
2602	0.7	(2,1,0)	[*BBBABBABBA*]
254	0.714286	(2,1,0)	[*BBBABBA*]

[a]Ground state.
[b]Ground state.
[c]There are other configurations degenerate with $\gamma 2$. Some are not superlattices.

work, the interactions were made dependent on the *local* concentration x, but with a different definition of the local concentration. In the present work, we used a different approach, where for a new larger set of first-principles-calculated configurations, we fit the Hamiltonian in Eq. (8) with the fitting parameters $J_{f,l}$. In other words, now we choose to fit the interactions $J(x)$. The results in Ref. 27 showed that the strained $In_xGa_{1-x}N$ alloy comprises ordered structures or $[n,m]$ superlattices formed by n planes of In followed by m planes of Ga, which were stable up to 1000 K. The alloy ground-state line showed that the composition $x \cong 0.5$, around $[3,3]$, was favored. Therefore, we can say that the calculations performed in Ref. 27 lead to the same qualitatively result —i.e., the formation of stable ordered structures around $x=0.5$, though, the most stable structure must be corrected to the $DO_{22}2/4$ structure.

Any configuration σ can be represented by a point $(x(\sigma),E(\sigma))$ in Fig. 3, even if it is above the GSL. Thus, in addition to the stable ordered structures, we also include in Fig. 3 some ordered configurations with energy very close to the GSL (a difference of less than 3 meV/cation). A list of configurations thus near the GSL is given in Table IV. As some configurations have no specific name, we named them according to the sequence number of our file with the 5868 different configurations. Most are (210)-oriented superlattices. Observe that, among the competing (210)-oriented superlattices of Table IV, none has more than three consecutive planes B. It is worth noting that the configuration representing the inflection point of the GSL at $x=0.625$ was not calculated by the LDA, and because there are many competitive (210)-oriented superlattices in the range $0.5 \leqslant x \leqslant 0.67$, including $\gamma 2$ itself, it is difficult to assert that this configuration is indeed belonging to the GSL. We mention that we tried other fits, excluding $\gamma 2$, and with 14 parameters J instead of 15, and the first inflection point was always the $DO_{22}2/4$ structure, while the second inflection point changed to a neighbouring (210)-oriented superlattice, one of those listed in Table IV. Thus, we infer that the straight line piece between the two representing mixtures of the two phases also represent (210)-oriented superlattices with intermediate concentrations. Therefore, we can say that the GSL is composed by the $DO_{22}2/4$ structure and another (210)-oriented superlattice in the range of composition $0.5 \leqslant x \leqslant 0.67$.

In the case of the unstrained alloys, we found that the GSL is only formed by the two pure binary constituents meaning there is no stable ordered phase in this case, and showing the tendency of the unstrained InGaN to phase separate. This finding is in agreement to other works in the literature.[12,16,17]

These results show that the coherence with the substrate greatly suppresses the tendency for alloys to separate into their pure-component "end-point" phases and, at same time, greatly enhances their tendency to form ordered compounds at certain stoichiometric compositions. In fact, some special ordered atomic arrangements can simultaneously accommodate two different bond lengths in the alloy in a coherent fashion and maximize charge transfer, hence becoming more stable, although ordering is sensitive to the growth conditions. Ordering occurs only in a determined temperature range because a minimum temperature is needed for the surface atoms to diffuse to their ordered positions while a higher temperature would tend to drive the system into the disordered phase.

Therefore, having identified the ground-state structures for the strained case, we intend to know if the $DO_{22}2/4$ structure has a large range of stability or not. Then, as explained before, it is useful to know the stability limit temperature T_c and if it is sufficiently high to allow growth of these ordered phases. For this purpose, we proceeded with the MC thermodynamics. We observed ordering via the intensity of the Bragg reflection peaks. Choosing $\vec{k} = (\pi/2)(210)$, which is in the direction of the superlattice repetition, the intensity for a perfect $DO_{22}2/4$ is

$$S(\vec{k})S(\vec{k})^* = \frac{N^2}{2} = \frac{(12^3)^2}{2} = 1\,1492\,992,$$

$$\vec{k} = \frac{\pi}{2}\begin{pmatrix} 2 \\ 1 \\ 0 \end{pmatrix} \quad \text{for perfect order}.$$

For other wave vectors $S(\vec{k})S(\vec{k})^*$ is small. As the temperature increases the value of this Bragg intensity decreases by orders of magnitude, and the background increases (as shown in Fig. 5), which means that the phase transition is near to occur. From the Bragg peak positions in the first Brillouin zone one unequivocaly identifies the ordered phase as $DO_{22}2/4$. In other words, the MC calculation confirms the ground-state search in that it also sets the configuration $DO_{22}2/4$ as the most stable at $x=0.5$.

As the temperature increases, we observe that the intensity of the Bragg lines has a continuous behavior. In our case, using the 27 entries of the last column of Table I and 15

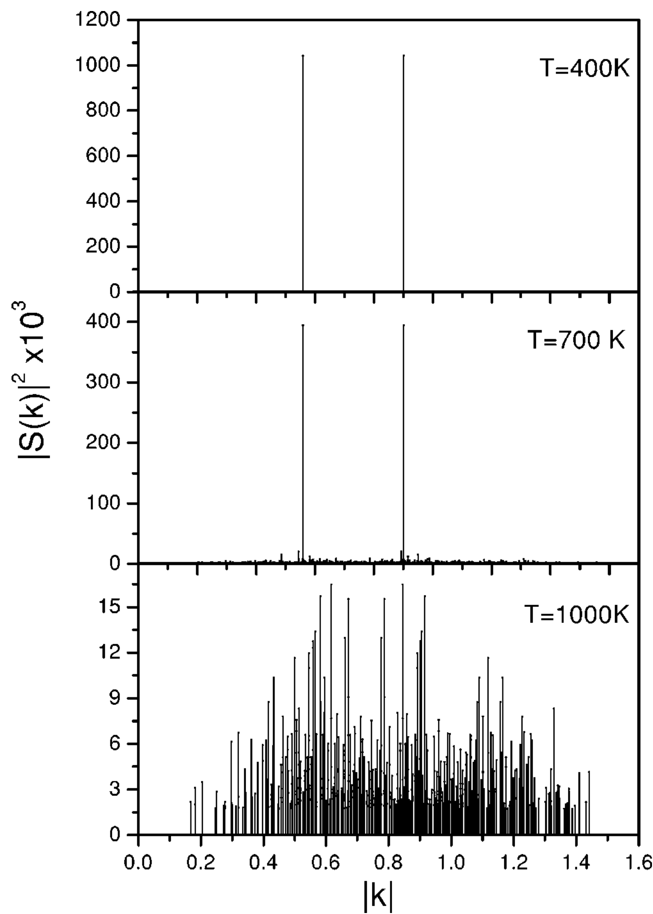

FIG. 5. Intensity of the Bragg lines for all $\vec{k}$ in the first Brillouin zone of the MC cell for three temperatures for the $In_{0.5}Ga_{0.5}N$ alloy. The two peeks observed for $T=400$ K and 700 K correspond to the $DO_{22}2/4$ structure.

interaction parameters we found a smooth transition from 0 K to about 1000 K with a inflection at 700 K, possibly indicating a first-order transition, although we cannot establish the exact value of the transition temperature. As the temperature decreases, the intensity as a function of temperature repeats its behavior in heating. This behavior is depicted in Fig. 6. The relatively small size of the MC cell might be responsible for the absence of hysteresis and a definite value for the transition temperature. Using 14 interaction parameters, instead of 15, and 25 fit configurations, instead of 27, the results were substantially the same. Then, we can conclude that strained c-$In_{0.5}Ga_{0.5}N$ has a stable $DO_{22}2/4$ phase with a broad enough temperature window of stability.

It is interesting to point out that there exists a large class of tetrahedrally bonded semiconductors with the $DO_{22}2/4$ structure for which the critical temperature is known to be very high.[47] In particular, for another system also with large size mismatch, the $GaAs_xSb_{1-x}$, it was predicted that the coherent epitaxy leads to the formation of the $DO_{22}2/4$-type ordered alloys.[26] For the $GaAs_{1-x}N_x$ alloys it was also found that the (111) and (100) directions are energetically less stable than the chalcopyrite structure, where the strain is maximally relieved by intermixing.[48]

We turn now to the already mentioned results of PL and HRXRD experiments on c-GaN/InGaN/GaN DH's where In-rich phases with composition of about 0.55 were observed in all analyzed samples.[14] The InGaN layers in the DH's were grown at 600 °C. The structures consisted of a 300-nm-thick buffer layer previously grown on a GaAs (001) substrate, a 30-nm-thick $In_xGa_{1-x}N$ layer with x in the range 0.09–0.33, and a 30-nm-thick GaN cap layer. To explain these experimental results it should be noted three aspects: (a) since the GaN layer, grown on GaAs (001) substrate, is 300 nm thick, it is observed to be relaxed meaning that it has its own lattice parameter; (b) the InGaN layer grown on GaN is strained, having the same parallel lattice constant as GaN, as in fact observed by the HRXRD measurements; [14] and (c) the observed In composition of the In-rich phase around 0.5 is very different from what was formerly predicted and observed for a fully relaxed InGaN layer ($x\sim0.8$).[17,49–53] Thus, our calculations indicate that the In-rich phases observed in these samples are mainly ordered $In_{0.5}Ga_{0.5}N$ domains of (210)-oriented superlattice structures with In concentration ranging from 0.5 to approximately 0.625. This is in agreement with the In contents, measured by HRXRD in these DH's, of about 0.55 instead of exact 0.5.

Although for h-InGaN layers ordered structures with In content 0.5 have been observed, ordering remains to be detected in the cubic modification of the alloy.

There are in the literature two theoretical methods commonly used for predictions of phase separation in group-III nitrides, the regular solution model[53] and the generalized quasichemical approximation.[17] Neither method provides any information about ordered phases. Dealing with ordering, to our knowledge so far, there are only two theoretical works, one by Shimotomai and Yoshikawa[54] and other by Northrup *et al.*[22] In the work of Shimotomai and Yoshikawa, one predicts atomic ordering in the In-rich precipitates for InGaN alloys by using a very simplified empirical model that does not include any strain effect. Its explanation for the ordering formation is based on higher-order pairwise interactions beyond first neighbors. The long-range pair interaction is an unlikely cause for ordering in semiconductors, as shown by Zunger, Wei, and Ferreira for various III-V semiconductors.[24–26,33] The inclusion of higher-order interactions can in fact lead to asymmetric phase diagrams,[17] but hardly ordering. The causes of ordering have been already extensively studied in the literature,[23–26,33] and three aspects are already well known: (a) bulk ordering, obtained from the contrast between the total energy of various assumed bulk ordered phases with those of the random phase, and its stability with temperature; (b) epitaxial ordering, where the coherence with the substrate can convert the previously predicted metastable/unstable bulk ordering into stable ordering; and (c) reconstruction-induced ordering, where the free surface can exhibit surface reconstructions leading to new stable structures *absent* both from bulk and epitaxial calculations (e.g., the CuPt ordered phase). In the work of Northrup *et al.*, the authors present first-principles calculations of the structure and energetics of the $GaN(10\bar{1}1)$ surface and models for the reconstructions. The authors proposed that the chemical ordering in h-InGaN is driven by the preference for In incorporation at the sites of reduced N coordination present at steps during growth on the (0001) and $(000\bar{1})$ surfaces. This

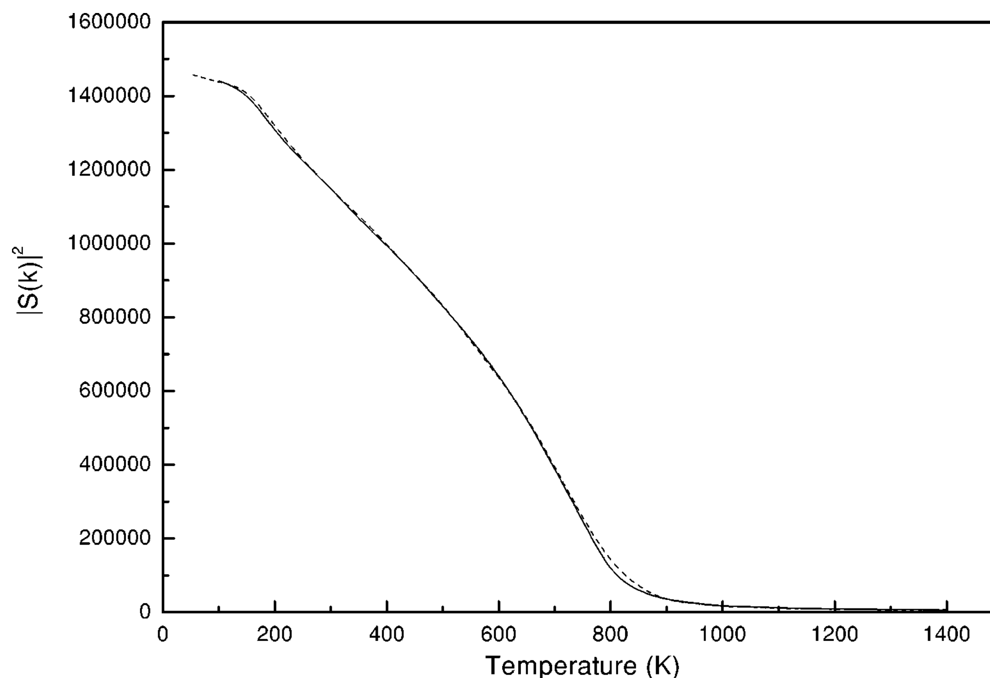

FIG. 6. Intensity of the Bragg line (210), representing the $DO_{22}2/4$ structure, as a function of temperature. The dashed line was obtained by cooling the MC sample from high temperatures. The solid line was obtained when heating the sample from perfect chacopyrite ($DO_{22}2/4$) order.

last aspect was not taken into account in our calculations. Although only considering the two first aspects cited above, (a) and (b), we could already predict the formation of ordered structures. Thus, we consider as a possible explanation for the In-rich phase with $(x\sim 0.5)$ observed in the experiments the formation of ordered structures, induced by the biaxial strain produced by the coherency between the layers of InGaN and GaN. The ordered phases thus induced are superlattices with ordering vector (2,1,0).

IV. SUMMARY

In conclusion, we have presented the results of a study of the energetics and thermodynamic properties of unstrained and strained ternary $In_xGa_{1-x}N$ epitaxial layers. We have combined a modified CE method with MC simulations and *ab initio* DFT-LDA calculations. In the strained alloy we observed ordered phases not present in the relaxed bulk material. According to the CE, the superlattices with ordering vector (2,1,0) are favored, the ground state being made of a chalcopyrite-like structure (alternation of [InInGaGa] along (210)) and another (210)-oriented superlattices with In concentration up to about 62.5%. The results indicate that the In-rich phases with In concentration around 0.55 recently observed experimentally are mainly ordered domains of (210)-oriented superlattice structures.

ACKNOWLEDGMENTS

We acknowledge fruitful discussions with Klaus Lischka. This work was supported by the Brazilian funding agencies FAPESP and CNPq.

*Corresponding author. Electronic address: kuhl@if.usp.br
†Electronic address: guima00@superig.com.br;
‡Electronic address: scolfaro@macbeth.if.usp.br
§Electronic address: jrleite@if.usp.br

[1] S. Nakamura and G. Fasol, *The Blue Laser Diode* (Springer, Berlin, 1997).
[2] O. Ambacher, J. Phys. D **31**, 2653 (1998).
[3] S. J. Pearton, J. C. Zolper, R. J. Shul, and F. Ren, J. Appl. Phys. **86**, 1 (1999).
[4] P. Kung and M. Razeghi, Opto-Electron. Rev. **8**, 201 (2000).
[5] *Data in Science and Technology: Semiconductors*, edited by O. Madelung (Springer-Verlag, Berlin, 1991).
[6] V. Yu. Davydov, A. A. Klochikhin, R. P. Seisyan, V. V. Emtsev, S. V. Ivanov, F. Bechstedt, J. Furthmüller, H. Harima, A. V. Mudryi, J. Aderhold, O. Semchinova, and J. Graul, Phys. Status Solidi B **229**, R1 (2002).
[7] J. Wu, W. Walukiewicz, K. M. Yu, J. W. Ager III, E. E. Haller, H. Lu, W. J. Schaff, Y. Saito, and Y. Nanishi, Appl. Phys. Lett. **80**, 3967 (2002).
[8] S. Chichibu, T. Azuhata, T. Sota, and S. Nakamura, Appl. Phys. Lett. **69**, 4188 (1996); **70**, 2822 (1997).
[9] K. P. O'Donnell, R. W. Martin, and P. G. Middleton, Phys. Rev. Lett. **82**, 237 (1999).
[10] C. Wetzel, T. Takeuchi, H. Amano, and I. Akasaki, J. Appl. Phys.

85, 3786 (1999).
[11] S. F. Chichibu, A. C. Abare, M. P. Mack, M. S. Minsky, T. Deguchi, D. Cohen, P. Kozodoy, S. B. Fleischer, S. Keller, J. S. Speck, J. E. Bowers, E. Hu, U. K. Mishra, L. A. Coldren, S. P. DenBaars, K. Wada, T. Sota, and S. Nakamura, Mater. Sci. Eng., B **59**, 298 (1999).
[12] V. Lemos, E. Silveira, J. R. Leite, A. Tabata, R. Trentin, L. M. R. Scolfaro, T. Frey, D. J. As, D. Schikora, and K. Lischka, Phys. Rev. Lett. **84**, 3666 (2000).
[13] I. L. Krestnikov, N. N. Ledentsov, A. Hoffmann, D. Bimberg, A. V. Sakharov, W. V. Lundin, A. F. Tsatsul'nikov, A. S. Usikov, Zh. I. Alferov, Yu. G. Musikhin, and D. Gerthsen, Phys. Rev. B **66**, 155310 (2002).
[14] O. Husberg, A. Khartchenko, D. J. As, H. Vogelsang, T. Frey, D. Schikora, K. Lischka, O. C. Noriega, A. Tabata, and J. R. Leite, Appl. Phys. Lett. **79**, 1243 (2001).
[15] M. K. Behbehani, E. L. Piner, S. X. Liu, N. A. El-Masry, and S. M. Bedair, Appl. Phys. Lett. **75**, 2202 (1999).
[16] S. Yamaguchi, M. Kariya, S. Nitta, H. Kato, T. Takeuchi, C. Wetzel, H. Amano, and I. Akasaki, J. Cryst. Growth **195**, 309 (1998).
[17] L. K. Teles, J. Furthmüller, L. M. R. Scolfaro, J. R. Leite, and F. Bechstedt, Phys. Rev. B **62**, 2475 (2000).
[18] A. Tabata, L. K. Teles, L. M. R. Scolfaro, J. R. Leite, A. Kharchenko, T. Frey, D. J. As, D. Schikora, K. Lischka, J. Furthmüller, and F. Bechstedt, Appl. Phys. Lett. **80**, 769 (2002).
[19] R. Singh, D. Doppalapudi, T. D. Moustakas, and L. T. Romano, Appl. Phys. Lett. **70**, 1089 (1997).
[20] D. Doppalapudi, S. N. Basu, K. F. Ludwig, Jr., and T. D. Moustakas, J. Appl. Phys. **84**, 1389 (1998).
[21] P. Ruterana, G. Nouet, W. Van der Stricht, I. Moerman, and L. Considine, Appl. Phys. Lett. **72**, 1742 (1998).
[22] J. E. Northrup, L. T. Romano, and J. Neugebauer, Appl. Phys. Lett. **74**, 2319 (1999).
[23] G. P. Srivastava, J. L. Martins, and A. Zunger, Phys. Rev. B **31**, R2561 (1985).
[24] L. G. Ferreira, S.-H. Wei, and A. Zunger, Int. J. Supercomput. Appl. **5**, 34 (1991).
[25] S.-H. Wei, L. G. Ferreira, and A. Zunger, Phys. Rev. B **45**, 2533 (1992).
[26] A. Zunger, *Handbook of Crystal Growth* (D. T. J. Hurle, Elsevier, Amsterdam, 1994), Vol. 3, p. 998.
[27] L. K. Teles, L. G. Ferreira, J. R. Leite, L. M. R. Scolfaro, A. Kharchenko, O. Husberg, D. J. As, D. Schikora, and K. Lischka, Appl. Phys. Lett. **82**, 4274 (2003).
[28] J. M. Sanchez, F. Ducastelle, and D. Gratias, Physica A **128**, 334 (1984).
[29] V. Ozoliņš, C. Wolverton, and A. Zunger, Phys. Rev. B **57**, 6427 (1998).
[30] Z. W. Lu, S.-H. Wei, A. Zunger, S. Frota-Pessoa, and L. G. Ferreira, Phys. Rev. B **44**, 512 (1991).
[31] D. de Fontaine, in *Solid State Physics*, edited by H. Ehrenreich, F. Seitz, and D. Turnbull (Academic, New York, 1979), Vol. 34, p. 73.
[32] J. W. D. Connolly and A. R. Williams, Phys. Rev. B **27**, 5169 (1983).
[33] L. G. Ferreira, S.-H. Wei, and A. Zunger, Phys. Rev. B **40**, 3197 (1989).
[34] A. A. Mbaye, L. G. Ferreira, and A. Zunger, Phys. Rev. Lett. **58**, 49 (1987).
[35] L. G. Ferreira, A. A. Mbaye, and A. Zunger, Phys. Rev. B **37**, 10 547 (1988).
[36] L. G. Ferreira, V. Ozoliņš, and A. Zunger, Phys. Rev. B **60**, 1687 (1999).
[37] P. Hohenberg and W. Kohn, Phys. Rev. **136**, B864 (1964).
[38] W. Kohn and L. J. Sham, Phys. Rev. **140**, A1133 (1965).
[39] D. Vanderbilt, Phys. Rev. B **41**, 7892 (1990).
[40] U. Großner, J. Furthmüller, and F. Bechstedt, Phys. Rev. B **58**, R1722 (1998).
[41] U. Großner, J. Furthmüller, and F. Bechstedt, Appl. Phys. Lett. **74**, 3851 (1999).
[42] J. P. Perdew and A. Zunger, Phys. Rev. B **23**, 5048 (1981).
[43] H. J. Monkhorst and J. D. Pack, Phys. Rev. B **13**, 5188 (1976).
[44] G. Kresse and J. Furthmüller, Phys. Rev. B **54**, 11 169 (1996).
[45] G. Kresse and J. Furthmüller, Comput. Mater. Sci. **6**, 15 (1996).
[46] N. Metropolis, A. W. Rosenbluth, M. N. Rosenbluth, A. H. Teller, and E. Teller, J. Chem. Phys. **21**, 1087 (1953).
[47] A. Zunger, Appl. Phys. Lett. **50**, 164 (1987).
[48] J. Neugebauer and C. G. Van de Walle, Phys. Rev. B **51**, 10 568 (1995).
[49] L. M. R. Scolfaro, Phys. Status Solidi A **190**, 15 (2002).
[50] E. Silveira, A. Tabata, J. R. Leite, R. Trentin, V. Lemos, T. Frey, D. J. As, D. Schikora, and K. Lischka, Appl. Phys. Lett. **75**, 3602 (1999).
[51] T. Saito and Y. Arakawa, Phys. Rev. B **60**, 1701 (1999).
[52] T. Takayama, M. Yuri, K. Itoh, T. Baba, and J. S. Harris, Jr., J. Appl. Phys. **88**, 1104 (2000).
[53] S. Yu. Karpov, MRS Internet J. Nitride Semicond. Res. **3**, 16 (1998).
[54] M. Shimotomai and A. Yoshikawa, Appl. Phys. Lett. **73**, 3256 (1998).